Tracking and characterization of highly deformable cloud structures

Christophe Papin[1], Patrick Bouthemy[1] Etienne Mémin[1], and Guy Rochard[2]

[1] Irisa/Inria, Campus Universitaire de Beaulieu, 35042 Rennes Cedex, France
name.surname@irisa.fr,
[2] Centre de Météorologie Spatiale, Météo France, Avenue de Lorraine, BP 147, 22302 Lannion, France

Abstract. Tracking and characterizing convective clouds from meteorological satellite images enable to evaluate the potential occurring of strong precipitation. We propose an original two-step tracking method based on the Level Set approach which can efficiently cope with frequent splitting or merging phases undergone by such highly deformable structures. The first step exploits a 2D motion field, and acts as a prediction step. The second step can produce, by comparing local and global photometric information, appropriate expansion or contraction forces on the evolving contours to accurately locate the cloud cells of interest. The characterization of the tracked clouds relies on both 2D local motion divergence information and temporal variations of temperature. It is formulated as a contextual statistical labeling problem involving three classes "growing activity", "declining activity" and "inactivity".

1 Introduction

The study of the life cycle of strong convective clouds (CC) is an important issue in the meteorological field. Indeed, such cold clouds often convey hard weather situations as pouring rains or even tornadoes. We aim at providing forecasters with new and efficient image processing tools in that context. We have addressed two major issues: tracking of cold cloud cells and characterization of their convective activity. To this end, we have developed two original methods exploiting both motion and photometric information. These methods can also be of interest beyond the meteorological domain.

Preliminary studies in the meteorological domain have already considered these issues [1, 3]. Since these meteorological phenomena are present in cold cloud systems, detection of strong convective cloud cells first involves a low temperature thresholding step in infrared images. In [1, 3], relevant cells are then isolated according to spatial properties (ellipticity factor, distribution of the spatial gradient of temperature, minimal area,...), and tracking simply results from the overlap between the prediction of the position of a cell detected at time $\tau - 1$, using the previously estimated displacement of its gravity center, and a cell extracted at time τ.

A commonly adopted strategy in computer vision to extract and to track complex objects in an image sequence is to exploit deformable models such as active contours [4, 9]. Starting from an initial position, and using external forces and internal constraints, the contour shape is modified toward the desired solution. However, results are highly sensitive to the initial conditions, and the considered scheme usually prevents from handling shape with significant protrusions. Moreover, topological transformations of the silhouette shape, as merging and splitting of parts, cannot be properly coped with. Different extensions to the active contour techniques have been developed to alleviate these drawbacks, such as introducing particle system [17], exploiting so-called "pedal" curves [18], taking into account region-based informations [10, 20]. However, these shortcomings associated to active contours have been elegantly and efficiently overcome by the Level Set approach introduced by Sethian and Osher [14, 16]. In this mathematical framework, the curve evolution is described through the evolution of an implicit higher-dimensional scalar function. The curve evolution is now described in a fixed coordinate system (Eulerian description) enabling the handling of topological changes. Such an approach or a related formalism has been already exploited in meteorological applications [5, 7, 19]. The tracking of large cloud structures is achieved in [7] following the ideas proposed in [11] to recover the minimal paths over a 3D surface. This method however requires to previously extract the cloud boundaries in the successive considered images. In [19], a particle system [17] is exploited and embedded in an implicit surface formulation. In [5], regions corresponding to convective clouds are extracted by first introducing posterior probabilities associated to the different cloud types. The curves then grow up from user-defined "seed points" to the salient contour shapes.

To make easier the localization of the curve in the next image of the sequence, it seems relevant to exploit motion-based information. The integration of dynamic information has thus been proposed in [6] and quite recently in [12, 15] by adding a motion-based term in the propagation function. Nevertheless, these last methods consider parametric motion models (i.e. 2D affine motion models) which are inappropriate in case of highly deformable structures present in fluid motion such as clouds. In that context, dense motion fields are required to describe the non-linear nature of the cloud motions. Besides, in [12, 15], motion information is in fact introduced to perform motion segmentation.

During its life cycle (growth, stability and decline), a convective cloud cell is likely to undergo different changes of topology such as merging with other neighbouring cells or splitting. Indeed, it seems quite appropriate to follow the Level Set formulation to detect and track these clouds in meteorological satellite images. We propose an original two-stage Level Set method to handle this tracking issue. It introduces the use of dense motion information in a first step acting as a prediction stage. Then, the accurate location of the cloud is achieved in a second step by comparing the local intensity values to an appropriately estimated global temperature parameter representative of the tracked cloud cell. This step can generate appropriate expansion or contraction forces of the evolving

contours to localize the boundaries of the cold clouds of interest. This is of primary importance since the predicted position of the cloud cells usually overlap the real ones. Then, to characterize the convective activity of these clouds, we consider the joint evaluation of the local divergence information contained in the 2D estimated velocity field, and of the temporal variations of temperature of the cloud cell points. This leads to qualify the convective activity level of the cloud cell corresponding to its degree of vertical evolution. The characterization stage is formulated as a contextual statistical labeling problem involving three classes: "'growing activity", "declining activity" and "inactivity".

The sequel of this paper is organized as follows. Section 2 outlines the main aspects of the Level Set formulation. Section 3 briefly describes how the cold clouds are primarily detected. In Section 4, we describe our Level Set-based method to track these cold cloud cells. Section 5 deals with the characterization of the convective cells. The efficiency and accuracy of the proposed scheme is demonstrated in Section 6 with results obtained on numerous difficult meteorological situations. Section 7 contains concluding remarks.

2 Level Set formulation

We briefly recall the main aspects of the level set formalism [16]. Let $\eta^i(s,t_0)$ be a set of N closed initial curves in $\mathbb{R}^2$ with $i \in [1,N]$. An implicit representation of these curves is provided by the zero-level set of a scalar function ψ, defined by $z = \psi(\boldsymbol{X}(s),t_0) = \pm d$, where d is the minimal signed distance from the image point, represented by vector $\boldsymbol{X}(s) = [x(s),y(s)]^T$, to the curves $\eta^i(t_0)$ (the convention is plus sign for a location outside the set of curves $\eta^i(t_0)$). In our case, function ψ corresponds to a 3D surface Γ. $\{\eta^i(s,t),\ i = 1,N\}$ is the family of curves generated by the successive zero-level sets of the surface $\psi(\boldsymbol{X}(s),t)$ moving along its normal directions $\boldsymbol{n} = \frac{\nabla\psi}{|\nabla\psi|}$. For a given level set of ψ, $\psi(\boldsymbol{X}(s),t) = C$, the speed function F at position $\boldsymbol{X}(s)$ represents the component of the vector $\frac{\partial \boldsymbol{X}}{\partial t}$ normal to $\eta^i(s,t)$. Let $F = \frac{\partial \boldsymbol{X}}{\partial t}.\ \boldsymbol{n}$. Deriving each member of equation $\psi(\boldsymbol{X}(s),t) = C$, and using the expressions of $\boldsymbol{n}$ and F, we obtain the Eulerian formulation of the evolution equation monitoring the successive positions of the surface Γ, evaluated over a fixed grid:

$$\psi_t + F|\nabla\psi| = 0 \tag{1}$$

where $\nabla\psi = (\frac{\partial\psi}{\partial x}, \frac{\partial\psi}{\partial y})$. After each propagation step of the surface Γ according to the speed function F which is given by an iterative numerical resolution scheme, the relation $\psi(\boldsymbol{X}(s),t) = 0$ yields the new position of the family of curves $\eta^i(s,t)$.

The definition of a particular application based on the Level Set approach involves the design of the speed function F.

3 Early detection and initialization

Before considering the tracking of cold cloud cells, let us briefly mention the early detection stage which provides us with the initial positions of curves of interest.

This preliminary detection stage consists in a classical temperature thresholding of the processed infrared satellite images to extract the colder clouds which may contain convective activity. In the very first image of the sequence, the initial curves are all given by the contours of each connected set of pixels with temperature values lower than a given threshold I_{th}. In the current image of the sequence, this procedure is only valid for newly appearing cold clouds. Indeed, if the detected cloud areas are included in already tracked cells, they are removed. For the already tracked cells, we consider as initialization the contours obtained in the previous image and denoted $\eta_{\tau-1}$ (let us note that τ will designate the "physical" time attached to the image sequence whereas t will be used in the evolution process corresponding to the Level Set formulation). Let us note that for convenience temperature and intensity will be assimilated in the sequel (in practice, we use calibrated equivalence tables).

4 Tracking of cold cloud structures

Solving the tracking issue leads to specify the speed function F introduced in equation 1.

The top of a convective cloud is characterized by a low temperature due to its high altitude as a result of vertical displacements, and by spatial intensity gradients of rather small magnitude in the heart of the cloud cell but generally more important in the vicinity of its boundaries. We exploit this a priori knowledge both in the preliminary detection step providing the initial zero level sets as described above, and in the definition of the speed function F. Since we are dealing with moving entities, it appears particularly relevant to exploit dynamic information too. Indeed, predicting the new position of the curves at the next instant brings more robustness (by preventing from false pairing) and more efficiency (by saving iterations and then computational load). Then, a motion estimation step is introduced. We only consider the regions delineated by the closed contours $\eta_{\tau-1}$ as the support of the estimation of the 2D motion field to be used. As stressed in the introduction, we need to compute a dense 2D velocity field. To this end, we have adopted a robust incremental estimation method described in [13], leading to the minimization of a non convex energy function. This energy function involves robust M-estimators applied to the data-driven term based on the optical flow constraint equation, and to a regularization term preserving motion discontinuities. This method combines a hierarchical multigrid minimization with a multiresolution analysis framework. This last point is of key importance to provide accurate estimates in case of cloud displacements of large magnitude which are likely to occur in this application. The estimation of the 2D apparent motion field within selected areas must not be corrupted by the surrounding motions of neighboring lower clouds. We have thus introduced an adaptive subdivision scheme of the image, supplying an initial block partition close to the selected areas. In order to obtain the final velocity field at full resolution, the final size of blocks at full resolution in the minimization process is pixelwise.

We have designed a function F composed of two distinct components, F_1 and F_2, related respectively to dynamic and photometric information. These components will act in a sequential way in the evolution of the tracked curves.

4.1 Dynamic component F_1

The first component F_1 of the speed function F takes into account motion information. It is defined by:

$$F_1(p) = \xi_\omega(p)\ F_{A1}\ \boldsymbol{\omega}(p).\ \boldsymbol{n}(p) - \epsilon\kappa \tag{2}$$

where ξ_ω represents a stopping factor related to the 2D estimated motion field $\boldsymbol{\omega}$ between time $\tau-1$ and τ. F_{A1} is a positive constant greater than one which allows us to speed up convergence. The second term depends on the surface curvature given by $\kappa = \text{div}\ \boldsymbol{n}$. It can be seen as a smoothness term whose influence on the evolving curve depends on the value of parameter ϵ.

F_1 component is considered in a first step and then the photometric component F_2 intervenes. F_1 makes evolve contours according to the projection of $\boldsymbol{\omega}$ on $\boldsymbol{n}$. This component provides a prediction to the photometric tracking step. Compared to a classical motion-based curve registration technique, this formulation allows us to handle in a well-formalized and efficient way problematic events such as splitting, merging, crossing of cloud cells.

The component F_1 is of particular importance in case of small cloud cells, whose apparent displacement magnitude is larger than the size leading to no overlap between two successive positions. Let us mention that their 2D apparent motion is also due to the motion of the surrounding medium, which explains that we can recover their motion using a multiresolution regularization method.

The 2D velocity vector $\boldsymbol{\omega}(p)$ can be used only on the zero-level set, i.e. on the image plane. Therefore, we exploit the geometric Huyghen's principle: the value of $\boldsymbol{\omega}(p)$ at point p is given by the one at pixel $\tilde{p}$ in the image plane, which is the nearest to p. We denote $\hat{\boldsymbol{\omega}}(p)$ the velocity vector exploited at point p given by the one computed at $\tilde{p}$.

Following the same principle, the stopping factor $\hat{\xi}_\omega$ denotes the global "extension" of ξ_ω defined over the whole domain of ψ. We define it as follows:

$$\hat{\xi}_\omega(p) = \delta\big[\Delta d_T(p) \leq |\hat{\boldsymbol{\omega}}(p)|\big] \tag{3}$$

where δ is the Kronecker symbol, $\Delta d_T(p) = \sum_{t=1}^{T} |\boldsymbol{d}_t(p)|$ and $\boldsymbol{d}_t(p)$ is the shift vector at pixel p induced by the implicit surface evolution at the t^{th} iteration (for a total of T iterations). The stopping factor is equal to one when the value of $\Delta d_T(p)$ is lower than $|\hat{\boldsymbol{\omega}}(p)|$ and zero otherwise. The contour is stopped as soon as a sufficient number of pixels verify $\hat{\xi}_\omega(p) = 0$. This stopping factor expresses the fact that the total shift applied to the evolving contour at a given point p must be bound by the magnitude of the corresponding estimated velocity vector.

If the hypersurface Γ at iteration $t-1$ is the signed distance to the contours $\eta(t-1)$. By using the Huyghen's principle, updating function ψ to give $\psi(t)$ turns

out to be similar for all pixels p_n of the grid belonging to the normal to $\eta(t-1)$ at pixel p. The intersection of the hypersurface Γ to the plane $(zO\boldsymbol{n})$ is indeed a straight line of slope unity. Finally, we can write $\boldsymbol{d}_t(p) = -\big(\psi_p(t) - \psi_p(t-1)\big)\boldsymbol{n}$. The contour shift at point p between iteration $t-1$ and t is effective if $\boldsymbol{d}_t(p) > \frac{1}{2}$, since the extraction process providing the current position of the contours after each iteration only yields entire coordinates. An example of results is shown on Figure 1.

4.2 Photometric component F_2

We aim at determining a strategy able to accurately move contours toward the real cold cloud boundaries. To this end, we exploit thermal information (i.e., intensity information in thermal infrared images) over contours. These local temperatures are compared to a global temperature characteristic of the tracked cloud cell at time τ. The sign of the difference of these local and global temperatures determines the way the contour evolves, i.e. the direction of the applied force F_2 at point p. This allows us to explicitly introduce locally contracting or expanding evolution of the contour according to the local configuration at hand, which is of particular importance since the current and desired positions of the curve are supposed to overlap. A somewhat similar flexible mechanism but issued from different considerations has also been proposed quite recently in [2] to extract shapes from background in static images.

The global characteristic temperature of the cloud cell at time τ is estimated as follows. It is predicted from dynamic and thermal information obtained from the previous time instant. We denote the characteristic temperature associated to the i^{th} contour η_τ^i at time τ by θ_i. θ_i is obtained by assuming that the intensity

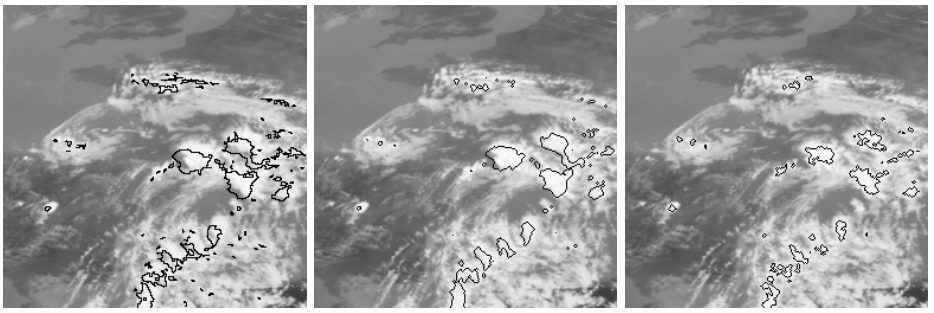

(a) (b) (c)

Fig. 1. Contour evolution successively monitored by the two components of the speed function F and their associated stopping factors. Part of infrared Meteosat image acquired on August 10, 1995 at 12h30 TU. (a) Initial contours (overprinted in black). (b) Contours after the first tracking step involving F_1 component. (c) Final contours after successively performing the two tracking steps involving respectively F_1 component and F_2 component.

function verifies the following continuity equation of fluid mechanics:

$$\frac{\partial I}{\partial \tau} + \text{div}(I\boldsymbol{\omega}) = 0 \tag{4}$$

This equation is related to the assumption that expansion or contraction of fluid (associated to a dissipation or to a concentration of matter) corresponds to intensity changes in the image sequence. Recalling that $\text{div}(I\boldsymbol{\omega}) = \boldsymbol{\omega}.\boldsymbol{\nabla} I + I\text{div}\ \boldsymbol{\omega}$, and using the expression of the total derivative of I with respect to time $\frac{dI}{d\tau} = \frac{\partial I}{\partial \tau} + \boldsymbol{\omega}.\boldsymbol{\nabla} I$, we can rewrite equation (4) as follows:

$$\frac{dI}{d\tau} + I\text{div}\ \boldsymbol{\omega} = 0 \tag{5}$$

Assuming, as in [8], a constant speed over the "particles" trajectories from $\tau - 1$ to τ, we can express intensity I at time τ at the displaced point $p + \boldsymbol{\omega}(p)$ by integrating both members of equation 5, which leads to:

$$I(p + \boldsymbol{\omega}(p), \tau) = I(p, \tau - 1)\ \exp\Big(-\text{div}\ \boldsymbol{\omega}(p)\Big) \tag{6}$$

The characteristic temperature θ_i of the cell corresponding to contour η_τ^i can be given by the mean of $I(p + \boldsymbol{\omega}(p), \tau)$ evaluated over region $\mathcal{R}_{\tau-1}^i$ delineated by the contour $\eta_{\tau-1}^i$:

$$\theta_i = \frac{1}{N_i} \sum_{p \in \mathcal{R}_{\tau-1}^i} I(p, \tau - 1)\ \exp\Big(-\text{div}\ \boldsymbol{\omega}(p)\Big) \tag{7}$$

where N_i is the number of pixels in $\mathcal{R}_{\tau-1}^i$.

We need to compute the divergence of the 2D estimated motion field. It is expressed by $\text{div}\ \boldsymbol{\omega}(p) = \frac{\partial u(p)}{\partial x} + \frac{\partial v(p)}{\partial y}$, where $\boldsymbol{\omega}(p) = [u(p), v(p)]^T$ is the velocity vector at pixel p. It is derived from the estimated motion field by using appropriate derivative filters.

Solving equation (1) leads to move the set of initial curves toward the new positions of cloud cells. We have designed the following expression of the speed function F_2 composed of a curvature term and a so-called advection term:

$$F_2(p) = \hat{\xi}_I(p)\ \overbrace{F_{A2}\ \text{sign}\Big(\theta_i - I(p)\Big)}^{\text{advection term } F_{adv}(p)}\ -\epsilon\kappa \tag{8}$$

where F_{A2}, θ_i and I respectively denote the constant magnitude of the advection force, the estimated characteristic temperature of the convective cloud cell i, and the intensity function in the infrared satellite image (intensity $I(p)$ here accounts for temperature).

As already mentioned, the definition of the advection term of F_2 allows us to deal with a force either of contraction or of expansion depending on the intensity value $I(p)$. This is further explained and emphasized below.

We need to exploit relevant image-based information to stop the evolution of the curves at the real boundaries of the cloud cells. To this end, we have to define a weighting factor in the speed function F_2, i.e. an image-based factor ξ_I, which will play the role of stopping criterion. The global "extension" of ξ_I, denoting $\hat{\xi}_I$, can be written as:

$$\hat{\xi}_I(p) = \max\Big(\delta[F^t_{adv}(p) + F^{t-1}_{adv}(p)], g_I(p)\Big) \tag{9}$$

where $\delta(x) = 0$ if $x = 0$, $\delta(x) = 1$ otherwise, function $g_I(p)$ is given by $g_I(p) = \frac{1}{(1+|\nabla G_\sigma * I(p)|)^2}$ and $F^t_{adv}(p)$ and $F^{t-1}_{adv}(p)$ respectively denote the advection term computed at times t and $t-1$. $\nabla G_\sigma * I(p)$ represents the convolution of the image with a Gaussian smoothing filter. When the evolving contours are located within warm areas (i.e. $I(p) > \theta_i$), they undergo a contraction force which moves them toward a cold cloud cell boundary. After a boundary of a cloud cell is crossed and the curve point is within the cloud cell, $I(p)$ becomes lower than θ_i. This induces a change of the sign of the advection term, and thus defines an expansion force. Since $\delta[F^t_{adv} + F^{t-1}_{adv}]$ becomes equal to 0, the value of $\hat{\xi}_I(p)$ is then given by $g_I(p)$ which can tend to zero if high intensity contrast is present at point p. Hence, we have introduced intensity spatial gradient information in an appropriate way, i.e. only when the evolving curve lies inside a cloud cell of interest. η^i_τ is now moving in the opposite direction, and stops by the first encountered contrasted intensity edges. Owing to the proposed scheme, evolving curves thus cannot be attracted by intensity edges belonging to non relevant clouds or to other visible structures in the image. An example of results obtained after performing successively the two tracking steps respectively involving components F_1 and F_2 is shown on Fig. 1c.

The use of both an appropriate initialization and a motion-based prediction embedded in the first tracking step allows us to provide a real tracking of convective cloud cells over time. We mean that we can effectively and reliably associate the extracted contours from one image to the next one, even in situations with no significant overlap between two corresponding contours.

To save computational time, we make use of the "narrow band" framework introduced in [14]. Moreover, we proceed each narrow band in an independent way. Then, if one of them contains a contour which has reached the desired cloud cell boundaries, the restriction of the function ψ to the corresponding narrow band is frozen, and the computational cost is thus further reduced.

5 Characterization of convective activity and extraction refinement

The clouds located within the closed contours η_τ issued from the tracking stage may include either truly active convective cell (CC), or CC in declining phase, or cold clouds which are not convective clouds. We have to identify regions undergoing strong vertical motion, corresponding either to growing or to declining

convective clouds. The vertical development of growing CC is accompanied with a spatial expansion at its top along with a temperature cooling. The opposite occurs for declining CC. Therefore, it seems particularly relevant, in order to qualify and to extract these convective activity areas, to jointly evaluate the degree of divergence of the 2D apparent motion and the tendency of the temporal changes in temperature.

5.1 Discriminant features of convective activity

The first discriminant feature of convective activity is related to the dynamic properties of the cold clouds of interest. It is supplied by the local divergence of the estimated 2D motion field, computed at each point of the tracked cloud cell as explained in Section 4.

The temporal evolution of the cloud temperature provides the second discriminant feature. We evaluate the temporal change of temperature at each point of the tracked cloud by considering the displaced frame difference supplied by the estimated 2D velocity field: $I_\tau(p, \boldsymbol{w}(p)) = I(p + \boldsymbol{w}(p), \tau) - I(p, \tau - 1)$. To take into account motion compensation errors and image noise, we consider in fact a locally average version:

$$\bar{I}_\tau(p, \boldsymbol{\omega}(p)) = \frac{1}{M} \sum_{r \in \mathcal{F}_p} \Big(I(r + \boldsymbol{\omega}(r), \tau) - I(r, \tau - 1) \Big) \tag{10}$$

where $\mathcal{F}_p$ is a local window centered on pixel p and containing M pixels. An example of joint evaluation of local motion divergence and temporal temperature variation can be found in Fig. 2. We can note the characteristic temporal evolution of a convective cloud cell (pointed with an arrow in images (a) and (d)).

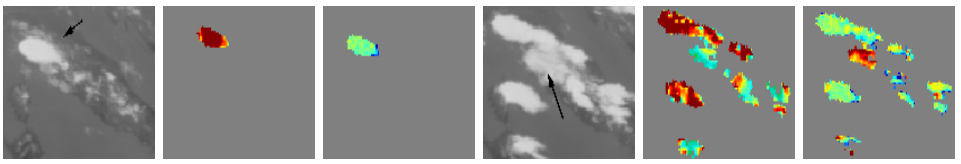

(a) (b) (c) (d) (e) (f)

Fig. 2. In columns (a) and (d), part of infrared Meteosat images acquired on August 4, 1995 at 11h00 TU and 13h30 TU. Local motion divergence maps (columns (b) and (e)), computed on convective cloud cells selected after the tracking stage, and the temporal variations of temperature (columns (c) and (f)). Display in Fig. b, c, e and f varies from light grey (highly negative values) to black (highly positive values).

The growing phase (Fig. 2a) presents strong positive values of motion divergence (dark grey in Fig. 2b) and a decrease in temperature (light grey in Fig.

2c). The subsequent declining phase (Fig. 2d) is identified by strong negative divergence values (light grey in Fig. 2e) and a warming up of the cloud top (dark grey in Fig. 2f).

5.2 Extraction of active convective clouds.

We have now to exploit these two discriminant features, i.e. div $\boldsymbol{\omega}(p)$ and $\bar{I}_\tau(p, \boldsymbol{w}(p))$, to determine the active convective clouds among the tracked cold cloud areas.

The CC characterization scheme is formulated as a labeling problem of these areas. We have adopted a contextual statistical approach based on Bayesian estimation (MAP criterion) associated with Markov Random Field (MRF) models. The MRF framework provides a powerful formalism to specify physical relations between observations o (i.e. temporal changes of temperature, local motion divergences) and the label field e, while easily allowing us to express a priori information on the expected properties of the label field (i.e. spatial regularization). We consider three classes, two classes of activity, growing activity ("*grow* ") and declining activity ("*decl* "), and one of inactivity ("*nact* "). The last one can contain non active clouds but also elements which remain undetermined due to non significant feature values.

Due to the equivalence between MRF and Gibbs distributions, it turns out that this leads to the definition of a global energy function $U(o, e)$. We have designed the following energy function composed of a data-driven term and a regularization term:

$$U(o, e) = \sum_{s \in \mathcal{S}} V_1(o, e) + \alpha_2 \sum_{c \in \mathcal{C}} V_2(e) \tag{11}$$

where V_1 and V_2 are local potentials, s is a site (here, a pixel), and $\mathcal{C}$ represents all the binary cliques c (i.e. cliques formed by two sites) associated with the considered second-order neighborhood system on the set of sites (pixels). α_2 controls the relative influence of the data-driven term and of the regularization term.

As a matter of fact, we consider the two features introduced above in a combined way through the following product:

$$\mu(s) = \operatorname{div} \boldsymbol{\omega}(s) \times \bar{I}_\tau\big(s,\ \boldsymbol{\omega}(s)\big) \tag{12}$$

The adequacy between a given label and the computed quantity $\mu(s)$ is governed by the sign and the magnitude of $\mu(s)$. If the two discriminant features present opposite signs at site s ($\mu(s) < 0$), this reveals convective activity, either growing activity ($\operatorname{div} \boldsymbol{\omega}(s) > 0$ and $\bar{I}_\tau < 0$) or declining one ($\operatorname{div} \boldsymbol{\omega}(s) < 0$ and $\bar{I}_\tau > 0$). To further distinguish labels "*grow* " and "*decl* ", we examine the sign of $\operatorname{div} \boldsymbol{\omega}(s)$. If $\operatorname{div} \boldsymbol{\omega}(s) < 0$, potential V_1 will favour the label "*decl* ", otherwise the label "*grow* " will be preferred. $\mu(s) > 0$ is not related to a specific physical meaning

and label "*nact*" will be favoured. The potential V_1 is defined at site s by:

$$V_1(o(s), e(s)) = \begin{cases} \text{sign}[\text{div } \boldsymbol{\omega}(s)] f(\mu) + \frac{1}{2} & \text{if } e(s) = grow \\ -\text{sign}[\text{div } \boldsymbol{\omega}(s)] f(\mu) + \frac{1}{2} & \text{if } e(s) = decl \\ -f(\mu) + \frac{1}{2} & \text{if } e(s) = nact \end{cases} \quad (13)$$

where $f(x)$ is a smooth stepwise function. We have chosen $f(x) = \frac{1}{\pi}\arctan(k\pi x)$. Potential V_2 in the regularization term is defined by $V_2[e(r), e(s)] = -\beta$ if $e(r) = e(s)$ and $V_2[e(r), e(s)] = \beta$ otherwise, where r and s are two neighbour sites. V_2 favours compact areas of same label. This formulation leads to the minimization of the global energy function $U(o, e)$, which is solved iteratively using the deterministic relaxation algorithm ICM.

The tracking process is concerned with all the cloud areas issued from the detection stage and not only with those from the characterization stage for the following reason. A large convective system can contain different zones of distinct activity which may evolve quickly over time. This temporal evolution does not allow us to perform a relevant and significant tracking of cloud cells displaying a real convective activity. Tracking cold clouds and characterizing in a second stage their convective activity appears to be more stable and physically more meaningful.

6 Results

We have carried out numerous experiments on real complex examples involving Meteosat infrared or water vapor images. Here, we report representative results obtained after each stage of the proposed scheme. Figures 3 and 4 illustrate the tracking stage, figure 5 the characterization stage.

For display convenience, pixels corresponding to low temperature will be represented by white intensities, and conversely. Figure 3 contains three different meteorological situations. For each, we supply the initial contours corresponding to the cold clouds detected in the previous image (central row) and the final locations of the cold clouds (lower row). We can observe that the tracking is quite accurate even in case of large displacements, (first example in the left column of Fig. 5) or in case of the formation of holes within a cloud cell (third example, in the right column of Fig. 3). Let us point out that forecasters are particularly interested by the accurate and reliable determination of colder areas of convective clouds, which are generally quite uniform. Thus, the stopping criterion we have designed stops the inner part of the evolving curve at the first encountered well-contrasted intensity edges. The consequence is that resulting contours may be located inside cloud cells.

Examples of tracking of cloud cells over time are shown in Fig. 4. We can point out the accuracy and the temporal coherence of the obtained results, which is of key importance for forecasters, depicting successive meteorological satellite images over Italy and Sardigna. These warm European areas (dark grey level) are the source of convective activity. At 10h30 TU, small cloud cells over Italy reach higher altitude and are correctly detected in time. They grow, merge,

and progressively other surrounding cells undergo the same process. At 14h00 TU (last column, last row), a convective cloud cell becomes too warm with respect to the characteristic temperature estimated from the previous image, and consistently disappears. The characterization of the convective activity of

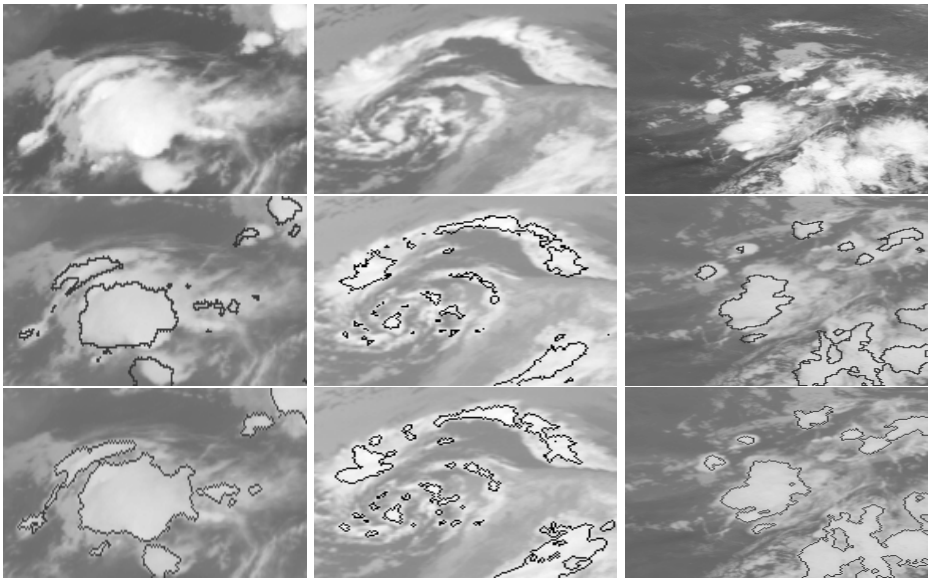

Fig. 3. Evolution of the cloud contours in the tracking stage. Upper row: original infrared images; central row: initial positions corresponding to those determined in the previous image; lower row: final positions of cloud contours. From left to right: part of Meteosat infrared images on August 24, 1995, at 18h30 TU, August 28, 1995, at 4h30 TU, and August 10, 1995 at 21h00 TU. Contours are overprinted in black.

the tracked clouds shown in Fig. 4 is reported on Fig. 5. Six successive results obtained after the characterization stage are supplied. Dark grey corresponds to active clouds in a growing phase. On the opposite, CC in a declining state are labeled in light grey. At the beginning of the sequence, the central cloud cell undergoes a strong vertical motion and the whole corresponding area is corrected labeled as "growing activity". Progressively, this cloud cell becomes less and less active, and the dark grey area shrinks toward its core. In the same time, a declining zone develops up to contain almost the entire area. The same parameter values are considered for all these experiments. Concerning the tracking stage, we set $F_{A1} = 10$, $F_{A2} = 10$, $\epsilon = 3$, and the width of the narrow band is 8 pixels. Temperature threshold I_{th} is $-35°C$. In the characterization stage, we set $k = 5$, $\beta = 0.1$ and $\alpha_2 = 3$. The choice of parameter values associated to the tracking stage only affects the speed of convergence and not the accuracy of results. Parameter values related to the characterization stage only influence the labeling of the uncertain activity areas (i.e. containing weak discriminant

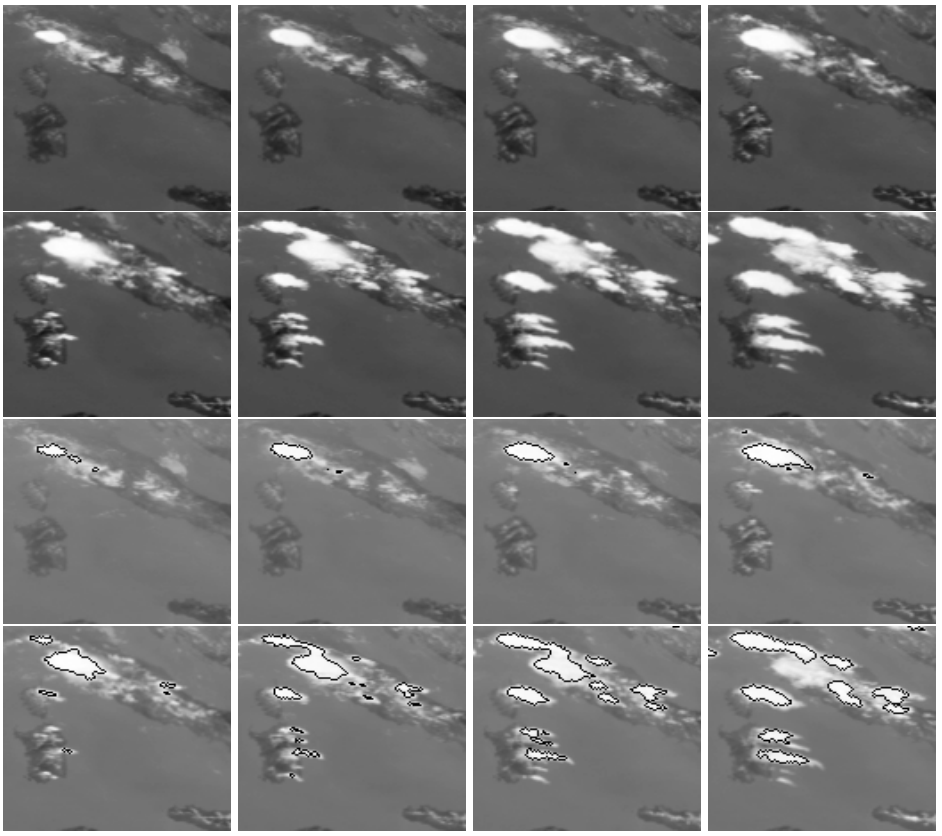

Fig. 4. Results of the tracking stage over a sequence of Meteosat infrared images (two first rows). Illustration of the temporal coherence of the tracking stage of cold clouds. Final contours are overprinted on the original images (two last rows). Part of Meteosat images acquired on August 4, 1995 from 10h30 to 14h00 TU.

feature magnitudes) and it was found that their setting was not critical. The tracking stage has been evaluated by forecasters on several real representative situations (including those reported in this paper) and appeared quite accurate. An extended experimental validation of the characterization stage is just about to be completed by a French meteorological center on the basis of a daily analysis by a forecaster in an operational context. First results are already convincing. The computational time is in accordance with operational requirements since Meteosat satellite images are acquired every thirty minutes. CPU time behaves as a linear function of the number of processed pixels (involved in the narrow band technique). It takes about six minutes for a quantity of processed pixels in the narrow bands equal to 128×128 on a Sun Ultra 60 workstation.

7 Conclusion

We have proposed in this paper an original and efficient framework to detect, track and characterize convective cold clouds from meteorological satellite im-

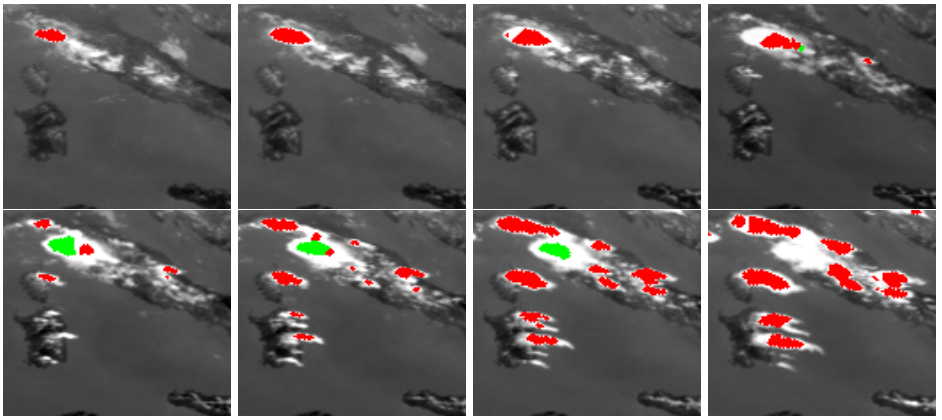

Fig. 5. Characterization stage applied to Meteosat infrared images. Labeling results are overprinted on the original images: in dark, resp. light, grey: growing, resp. declining, convective clouds. Part of Meteosat images acquired on August 4, 1995 from 10h30 TU to 14h00 TU.

ages. It involves two main stages, the tracking stage relying on the Level Set formalism, and the characterization stage stated as a statistical contextual labeling issue. This approach is quite relevant to properly process such highly deformable structures which are often subject to splitting or merging phases during their life cycle. We have designed a two-step tracking scheme exploiting both motion and photometric information in an adequate way. The first step exploits a 2D estimated motion field, and supplies a proper prediction to the second one. The former moves contours along the direction of estimated motion while immediately taking into account topological changes contrary to a usual registration step. The second step uses photometric information at a local level and at the cell level, and can create appropriate expansion or contraction forces on the evolving contours to accurately localize in every image the cold clouds of interest.

The characterization stage relies on local measurements involving divergence computed from the estimated 2D motion field and local temporal variations of the tracked clouds. It leads to the minimization of an energy function comprising a spatial regularization term. It allows us to extract, within the clouds delimited in the tracking stage, the regions of significant vertical motion, i.e. the really active convective cloud cells and to distinguish those in a growing phase from those in a declining phase. The computational time, which is usually a drawback of the Level Set approach, is significantly reduced, thanks to the two-step tracking scheme introduced in our method. Besides, the first tracking step, appropriately exploiting motion information, leads to positions of the curve overlapping the real boundaries of the cold clouds of interest. The second tracking step can then start from this prediction since the designed associated speed function allows a curve to evolve in two ways, contraction and expansion. Another advantage of this method is that results do not strongly depend on the choice of the parame-

ter values. Results obtained on numerous difficult real examples demonstrate the temporal coherence and the accuracy of the extracted convective clouds tracked over time, which provides forecasters with an easily understanding of the meteorological situation. Finally, the tracking method introduced in this paper is not specific to the considered application, and could be successfully applied to other kinds of deformable structures.

References

1. Adler, R.F., Negri, A.J.: A satellite infrared technique to estimate tropical convective and stratiform rainfall. J. Appl. Meteor. **27** (1988) 30–51
2. Amadieu, O., Debreuve, E., Barlaud, M., Aubert, G.: Inward and outward curve evolution using level set method. In Proc. of IEEE ICIP, Kobe, September (1999).
3. Arnaud, Y., Desbois, M., Maize, J.: Automatic tracking and characterization of convective systems on Meteosat pictures. J. Appl. Meteor. **1** (1992) 443–493
4. Blake, A., Isard, M.: Active contours. Springer (1998)
5. Brewer, M., Malladi, R., Pankiewicz, G., Conway, B., Tarassenko, L.: Methods for large scale segmentation of cloud images. In Proc. Meteorol. Satellite Data Users' Conf., Bruxelles (1997) 131–138
6. Caselles, V., Coll, B.: Snakes in movement. SIAM J. Numer. Anal., **3(6)** (1996) 2445–2456
7. Cohen, I., Herlin, I.: Tracking meteorological structures through curve(s) matching using geodesic paths. In Proc of 6th IEEE ICCV, Bombay, January (1998) 396–401
8. Corpetti, T., Mémin, E., Pérez, P.: Estimating Fluid Optical Flow. In Proc. of ICPR'2000, Barcelona, September (2000)
9. Kass, M., Witkin, A., Terzopoulos, D.: Snakes: Active contour models. IJCV **1** (1988) 321–331
10. Kervrann, C., Heitz, F.: A hierarchical markov modeling approach for the segmentation and tracking of deformable shapes. Graphical Models and Image Processing **60** (1998) 173–195
11. Kimmel, R., Amir, A., Bruckstein, A.M.: Finding shortest paths on surfaces using level sets propagation. IEEE Trans. on PAMI **17(6)** (1995) 635–640
12. Mansouri, A.R., Konrad, J.: Motion segmentation with level sets. In Proc of IEEE ICIP, Kobe, Japan, September (1999)
13. Mémin, E., Pérez, P.: A multigrid approach for hierarchical motion estimation. In Proc of 6th IEEE ICCV, Bombay, January (1998) 933–938
14. Osher, S., Sethian, J.A.: Fronts propagating with curvature dependent speed: Algorithms based on Hamilton-Jacobi formulation. Journal of Computational Physics **79** (1988) 12–49
15. Paragios, N., Deriche, R.: Geodesic active regions for motion estimation and tracking. In Proc of IEEE ICCV, Kerkyra, Greece, September **1** (1999) 688–694
16. Sethian, J.A.: Level Set Methods. Cambridge University Press (1996)
17. Szeliski, R., Tonnesen, D.: Surface modeling with oriented particle systems. Computer Graphics, SIGGRAPH, **26(2)** (1992) 185–194
18. Vemuri, B.C., Guo, Y.: Snake pedals: Geometric models with physics-based control. In Proc of 6th IEEE ICCV, Bombay, January (1998) 427–432
19. Yahia, H.M., Berroir, J-P., Mazars, G.: Fast and robust level-set segmentation of deformable structures. In Proc. IEEE ICASSP, Seattle, May (1998)
20. Zhu, S.C., Yuille, A.: Region competition: Unifying snakes, region growing, and Bayes/MDL for multiband image segmentation. IEEE Trans. on PAMI **18** (1996) 884–900